

Comparing the extended depth-of-field imaging performance of spherical aberration and asymmetric wavefront coding

Dirk Robinson and David Stork

Ricoh Innovations, Menlo Park CA

dirkr@rii.ricoh.com

Abstract: We compare the image quality between asymmetric wavefront codings and the simple-to-manufacture spherical aberration over an extended focal range. We verify and explain the superior performance of the spherical aberration via simulation results.

© 2009 Optical Society of America

OCIS codes: (060.2320) Fiber optics amplifiers and oscillators; (060.4510) Optical communications

1. Introduction

The last decade has seen numerous approaches to designing digital-optical imaging systems by analyzing and optimizing both the optics and digital image processing in a joint fashion [1, 2]. CDM Optics pioneered the concept of *wavefront coding* in which specially-designed phase plates are added to optical imaging systems to shape the wavefront at exit pupil thereby making optical magnitude transfer functions (MTF) that were practically *invariant* to depth. The images produced by such optical systems are but produced blurry images which are subsequently sharpened via digital image processing [3]. Subsequent researchers identified several classes of wavefront coding functions [4, 5] for extending the depth-of-field. All of these approaches are similar in the sense that the wavefront is explicitly controlled by phase plate added to the optical system for the purpose creating depth-invariant MTFs.

In this paper, we examine the extended depth-of-field imaging performance for *spherical coded* systems that leverage spherical aberration and digital processing to enable extended depth-of-field (EDoF) imaging. Spherical coding enjoys several important advantages over other wavefront coding techniques. First, the spherical aberration is imparted using standard rotationally-symmetric lens surfaces. Such surfaces are easy to design, manufacture and test. In fact, most optical design software tools enable direct control over the primary aberrations during system optimization. Second, the design eliminates the need for additional elements added to the optical system which add complexity and cost to a system. Third, the contrast preservation does not introduce the depth-dependent image spatial shifting associated with the asymmetric coding functions. Spherical aberration's ability to preserve high spatial frequencies through a large focal volume has been known for a while [6]. Recent research has demonstrated controlled application of spherical aberration for EDoF imaging applied to microscopes [7].

In this paper, we demonstrate that spherical coding also provides superior EDoF image quality throughout the focal volume in terms of mean square error (MSE) performance compared to the asymmetric aspheric wavefront coding approaches. We briefly review both the wavefront coding and spherical coding concepts and then compare their EDoF performance based on simulation. We then verify the extended depth-of-field imaging capabilities of spherical coding using an experimental system.

2. EDoF imaging through aperture coding

Both spherical coding and wavefront coding achieve extended depth-of-field (EDoF) imaging by designing an optical system with a particular optical path difference (OPD) or wavefront error function at the exit pupil of the optical system. For the purpose of this report, we examine wavefront error functions for on-axis field points, circular pupils, and assume approximate spatial-invariance of the point-spread-functions (PSF). The general form for wavefront function is $\Psi(\rho, \theta, W_{02}, \alpha) = W_{02}\rho^2 + \alpha c(\rho, \theta)$ which comprises a defocus term $W_{02}\rho^2$ and an aperture coding function $\alpha c(\rho, \theta)$ where ρ, θ are the normalized polar pupil coordinates (radius, angle), and W_{02} is the coefficient of defocus. The α term defines the strength of the aperture coding function. In this report, we compare three different coding functions. The functions are

$$c_w(\rho, \theta) = (\rho \cos \theta)^3 + (\rho \sin \theta)^3 \quad (1)$$

$$c_p(\rho, \theta) = \rho^3 \cos 3\theta \quad (2)$$

$$c_s(\rho, \theta) = \rho^4. \quad (3)$$

The first term is the original asymmetric wavefront coding function described by CDM Optics [3]. The second is a variant of the original wavefront coding function which we call *petal coding*. The third is the spherical coding function based on the Seidel spherical aberration. Both the first and second functions are based on odd-ordered polynomials characteristic of the majority of wavefront coding functions.

The optical transfer function (OTF) of the optical system is related to the OPD function according to the diffraction integral which is approximated

$$H(\omega, \nu, W_{02}, \alpha) = \mathcal{F}\{|\mathcal{F}\{A(\rho, \theta)e^{j2\pi\Psi(\rho, \theta, W_{02}, \alpha)}\}|^2\}, \quad A(\rho, \theta) = \begin{cases} 1, & \rho \leq 1 \\ 0, & \rho > 1 \end{cases}, \quad (4)$$

where $A(\rho, \theta)$ is the amplitude transmittance function of the exit pupil, \mathcal{F} the Fourier transform operator, and ω, ν the spatial frequencies [8]. For the purposes of this paper, we normalize these spatial frequencies by the diffraction-limited spatial frequency.

The original wavefront coding functions c_w and c_p were designed to minimize the MTF variation through a range of defocus values [3, 5] to create depth invariant MTFs. The odd-ordered wavefront coding functions enable the optical system to achieve very uniform MTF throughout the focal volume for many spatial frequencies. The MTF is restored by applying a digital sharpening filter to restore contrast. The digital filter has response $R(\omega, \nu)$. In the original wavefront coding papers $R(\omega, \nu)$ represents a linear inverse filter for restoring the depth-invariant MTF to that equivalent to an aberration-free optical system.

In our work on digital-optical design we use a global image quality measured based on mean-squared error (MSE) [2]. The MSE function combines image quality errors due to loss of contrast (bias) and those due to noise amplification (variance). In the case of extended depth-of-field imaging, we use an EDoF MSE figure of merit. We implicitly define the depth range in units of waves of the defocus aberration $W_{02} \in [-D, D]$. The MSE over the depth range is given by

$$MSE(D, \alpha, R) = \frac{1}{2DU^2} \int_{|W_{020}| < D} \int_{|\omega|, |\nu| < U} S(\omega, \nu) |H(\omega, \nu, W_{02}, \alpha)R(\omega, \nu) - 1|^2 + \sigma^2 |R(\omega, \nu)|^2 \quad (5)$$

where $S(\omega, \nu)$ represents the power spectral density (PSD) of the image signal and σ^2 represents the power of the noise in the captured images. We implicitly assume that the PSD is defined in terms of angular frequency in the object space mean that the same PSD function $S(\omega, \nu)$ applies independent of the object depth.

The integration limits over the spatial frequencies U reflect the *undersampling factor* of a digital-optical imaging system. The undersampling factor is the ratio between the Nyquist frequency of the digital detector ω_n over the diffraction-limited spatial frequency ω_d . For example, an $F\#4.0$ system at $0.5 \mu\text{m}$ wavelength with $10 \mu\text{m}$ pixels will have an undersampling factor of $U = \frac{50lp/mm}{500lp/mm} = 0.1$. Very often, digital-optical imaging systems have low undersampling factors ranging from 0.05 to 0.20 in order to maximize the amount of light hitting the detector.

After some algebraic manipulation, we find the linear filter minimizing the EDoF MSE of Eq. 5 has the spectral response

$$R(\omega, \nu, D, \alpha) = \frac{S(\omega, \nu)\bar{H}^*(\omega, \nu, D, \alpha)}{S(\omega, \nu)\check{H}^2(\omega, \nu, D, \alpha) + \sigma^2} \quad (6)$$

where

$$\bar{H}(\omega, \nu, D, \alpha) = \frac{1}{2D} \int_{-D}^D H(\omega, \nu, W_{02}, \alpha) dW_{02} \quad (7)$$

$$\check{H}^2(\omega, \nu, D, \alpha) = \frac{1}{2D} \int_{-D}^D |H(\omega, \nu, W_{02}, \alpha)|^2 dW_{02}. \quad (8)$$

Insert this EDoF Wiener filter into Eq. 5 we obtain the predicted EDoF MSE as

$$MSE(D, \alpha) = \frac{1}{U^2} \int_{|\omega|, |\nu| < U} \frac{S(\omega, \nu)\sigma^2 + S^2(\omega, \nu) [\check{H}^2(\omega, \nu, D) - \bar{H}^2(\omega, \nu, D)]}{S(\omega, \nu)\check{H}^2(\omega, \nu, D) + \sigma^2} \quad (9)$$

From Eq. 9, we see that the predicted MSE depends on two components. The first relates to the image quality using the average of the MTF over the depth volume. The second term is proportional to the variance of MTF over the depth range $[\check{H}^2(\omega, \nu, D) - \bar{H}^2(\omega, \nu, D)]$. In the case of wavefront coding, this second term is very small wavefront as the MTFs are nearly depth-invariant.

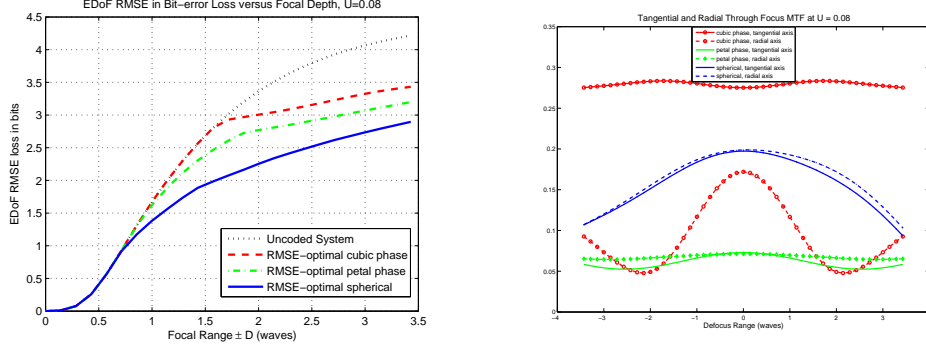


Fig. 1. The left graphs compare the EDoF RMSE for the three different aperture coding functions optimally scaled to minimize EDoF MSE (in bit loss) as a function of the focal depth $\pm D$. The spherical coding (blue solid) shows superior EDoF RMSE compared with the two asymmetric wavefront coding approaches (red dashed and green dash-dot). The right graph compares the through-focus MTF for the three coding functions for a tangential spatial frequency ($\nu = U$) and radial frequency ($\omega = \nu = \frac{U}{\sqrt{2}}$).

3. Simulation results

In this section we compare the EDoF MSE for the three different coding strategies as a function of focal depth range. We examine the MSE over an increasing depth range for a space of undersampling factors. We find that for many practical imaging systems, the undersampling factors range from about 0.05 to about 0.25. We explore the MSE performance over increasing depth ranges from $D \in [0, 3.5]$ waves of defocus. For each defocus range D , we optimally select the aperture coding strength coefficient $\alpha_i(D)$ which minimizes the MSE for the particular coding function. Also, for the spherical coding, we select the best center focus position which minimizes MSE experimentally. For our simulation experiments, we assume a flat PSD with $S(\omega, \nu) = 1$ and that the noise power is $\sigma^2 = 0.001$ (SNR of 30 dB). This PSD assumption reflects the total information throughput of the digital-optical system without any special tailoring to a particular class of image signals.

The left graph of Fig. 1 compares the EDoF MSE performance of the three different aperture coding strategies as a function of the size of the depth range $\pm D$ for a system with undersampling factor $U = 0.08$. We plot the EDoF MSE performance in log units as bits of error lost with respect to a theoretical Z-scan multiframe aberration free optical system capturing focussed optical images at every depth plane in the focal range. Up to about $\pm D = 0.75$ waves, the system is optimal without coding as the optical system is operating in the paraxial regime where the PSF is smaller than the pixel size. For larger focal volumes, all three coding strategies improve performance over an uncoded system, but the spherical coding system (solid) shows significant improvement over the asymmetric coding functions (dashed, dash-dotted). In other words, the spherical coding system, without any special optics, produces better image quality throughout the depth cube than both the other two coding strategies.

The reason for improved performance of the spherical coding over the asymmetric wavefront coding functions is explained by the wavefront coding goal of focus invariance. For example, the right graph of Fig. 1 compares the through-focus MTF for spatial frequencies along the tangential axis ($\nu = 0.08$) and along the radial axis ($\omega = \nu = \frac{0.08}{\sqrt{2}}$) for the three coding functions. The cubic-phase tangential through-focus MTF is very flat throughout the focal depth and has good contrast ($|H(0, \nu)| = 0.3$). The radial performance, however, is considerably worse both in constancy and MTF value. In other words, the standard cubic-phase shows excellent performance on the tangential and sagittal axes, but very poor performance along radial axes. The petal coding function makes the performance nearly rotationally symmetric as evidenced by the overlap between the solid and dashed green curves. This angular uniformity in MTF performance is achieved by sacrificing the general MTF level. The spherical coding system is naturally rotationally symmetric, but also, shows improved average MTF performance over the petal coding. The through-focus curve, however, is not as flat as the wavefront coding approaches. The spherical coding system achieves better MTF, and hence better EDoF MSE by sacrificing the constancy of the MTF throughout the focal depth. The depth-dependent variation in MTF of spherical coding is most apparent at lower spatial frequencies.

The spherical coding also achieves superior performance by making one additional sacrifice; namely, large point spread functions. The graphs of Fig. 2 compare the MTFs of the three different aperture functions along and radial axes ($\omega = \nu$) for systems up to an undersampling factor $U = 0.08$ at the paraxial image plane. The spherical coding

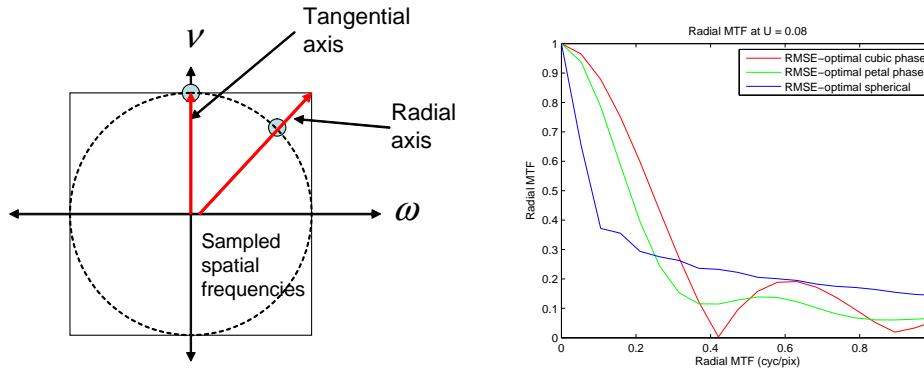


Fig. 2. The graph on the left shows the tangential and radial MTF axes. The right graph compares the MTF for the three coding functions along the radial axis ($\omega = \nu$) at the paraxial focus plane up to $U = 0.08$. The spherical coding curve (blue) shows poorer low frequency MTF, but better mid and high spatial frequency MTF than both wavefront coding functions along the radial axis.

has much lower MTF for low spatial frequencies, but better MTF for mid and high spatial frequencies. Since the mid and high spatial frequencies comprise a larger percentage of the total system bandwidth, the spherical coding provides superior EDoF MSE throughout the focal range. The lower MTF for low spatial frequencies requires reconstruction FIR filters with larger spatial extent. Essentially, this places increased burden on the digital subsystem in the digital-optical system. Most likely, this is explained by the higher-order polynomial used in the aperture coding function.

4. Conclusion

We demonstrate the superior extended depth-of-field (EDoF) MSE performance, and hence general imaging bandwidth, of spherical coding over the asymmetric wavefront coding functions. The spherical coding achieves better imaging quality by sacrificing MTF variation through the focal depth and by having larger point spread functions and hence requiring larger FIR filters. These results suggest several possible directions for future research. The spherical coding approach was developed as a very low-cost and easy-to-design method for achieving EDoF imaging systems. The aperture coding function was not designed to minimize EDoF MSE. Future work might find alternate aperture coding functions which can both improve EDoF MSE while at the same time minimize the FIR filter size requirements. Such aperture coding functions will most likely require aspheric lens surfaces, but might provide a nice tradeoff with respect to digital filter complexity. Also, future work could address the fundamental performance limitations on such single snapshot EDoF imaging system performance in terms of MSE.

References

1. W. T. Cathey and E. Dowski, "A new paradigm for imaging systems," *Applied Optics* **41**, 6080–6092 (2002).
2. D. G. Stork and M. D. Robinson, "Theoretical foundations for joint digital-optical analysis of electro-optical imaging systems," *Applied Optics* (2008).
3. E. Dowski and W. T. Cathey, "Extended depth of field through wave-front coding," *Applied Optics* **41**, 1859–1866 (1995).
4. W. Chi and N. George, "Electronic imaging using a logarithmic asphere," *Optics Letters* **26** (2001).
5. P. Pauca, R. Plemmons, S. Prasad, T. Torgersen, J. van der Gracht, and C. Vogel, "An Integrated Optical-Digital Approach for Improved Image Restoration," *Proceedings AMOS Technical Conference, Maui, HI* (2003).
6. G. Black and E. Linfoot, "Spherical aberration and the information content of optical images," *Proceedings of the Royal Society of London* **239**, 522–540 (1957).
7. P. Mouroulis, "Depth of Field Extension with Spherical Optics," *Optics Express* **16**, 12 995–13 004 (2008).
8. J. W. Goodman, *Introduction to Fourier Optics* (McGraw-Hill, New York, NY, 1986), second edn.